IOSR Journal of Mechanical and Civil Engineering (IOSR-JMCE)
e-ISSN: 2278-1684,p-ISSN: 2320-334X, Volume 16, Issue 6 Ser. I (Nov. - Dec. 2019), PP 45-57
www.iosrjournals.org

Seismic Behaviors of Steel/Concrete Composite Edge Beam-Column Joints under Cyclic Loading

Khaled Z. Sayed[1], Mohamed M. Salem[2]
[1] *Associate Professor of Reinforced concrete, Housing and Building National Research Center, Giza- Egypt*
[2] *Associate Professor of Reinforced concrete, Housing and Building National Research Center, Giza- Egypt*
Corresponding Author: Khaled Z. Sayed

Abstract : *This paper presents an experimental investigation on the behavior of steel-concrete composite edge joints under cyclic loading. Six specimens of edge composite beam-column joints have been tested to study the effect of different types of steel sections connection in the joint zone on the seismic behavior of structure members. The experimental parameters include concrete-encased composite columns with IPE (I) and Pipe (P) steel sections, As well as, concrete-encased composite beams with both built up (T) and (I) sections with equal/unequal flange width. The seismic behavior of edge joints such as failure mode, hysteresis curve, strength degradation, ductility and energy dissipation ability were investigated. Based on experimental results, all composed joints had shear failure mode at end of encased steel sections in the beam, due to sudden change of beam stiffness. Tinny cracks are detected at composed joint zone. The samples with encased I section had higher ultimate loads by 4.5% than control sample. Compared to maximum displacement of control specimen, joint of beams with encased I section gives higher displacement ratio than beams with encased T section. Joints of beams with encased I and T shaped steel section have good energy dissipation capacity than joint of both beams with narrow T flange width, and beams with cutting bars. Finally, it was concluded that, joints with composite steel sections minimize the cracks, and lead to weak beam-strong column criteria, as well as, improves its seismic behavior.*

Keywords : *Composite Edge joint ; Steel−Concrete composite edge joint ; Energy dissipation of edge joint ; Ductility of edge joint ; Seismic resistance of joint.*

Date of Submission: 26-10-2019 Date of Acceptance: 12-11-2019

I. Introduction

For conventional reinforced concrete frame structures, the seismic performance mostly depends on the ability of beams, columns and their joint zones to maintain substantial inelastic deformations without a significant loss of load carrying capacity. The beam-column joints are designed to sustain vertical loads, and horizontal loads from earthquake/wind. Evidence from recent earthquakes showed beam-column joints with insufficient transverse steel reinforcement often failed by brittle shear failure with 'x' shape cracks under reversed cyclic loading during the earthquake, [1 to 6], as shown in Fig. (1). As mentioned in both ACI318-14, and Kosh [1,7, &8], the joint shear strength is provided mainly by a diagonal compression strut that develops across the joint. The strut is effective in resisting shear under force reversals, if the joint aspect ratio h_{beam} / h_{column} (beam depth /column width in shear direction) is close to one. Therefore, additional transverse reinforcement might be required to support development of concrete strut, as shown in Fig. (2). From past researches, Waston et al. [9], mentioned that, transverse steel reinforcement serves as confinement of the concrete core and premature buckling of longitudinal steel reinforcement. Finally, it leads to enhancement of shear capacity in the joint zone. However, an increased amount of transverse steel reinforcement in the joint zone will producing difficulties in both arranging steel bars and the compactness of concrete due to dense shear reinforcement ratio. Pan, et al.[5], concluded that, increase of the axial load on the column cannot increase the ultimate load capacity and ductility since they all failed by flexural failure at the base of the beam, but can result in increased ductility coefficient because the additional axial load can restrain propagation of cracks in the joint specimen. Therefore, the parameters such as, reinforcing joint zone by additional transverse steel reinforcement, and effect of increasing axial loads, (20% to 30% of column carrying capacity), on the column on improvement the ductility of composite joint, were taken based on previous researches results and code requirements.

Fig. 1: Failure-of-corner-beam-column-joints-in-Izmit-earthquake-in-Turkey

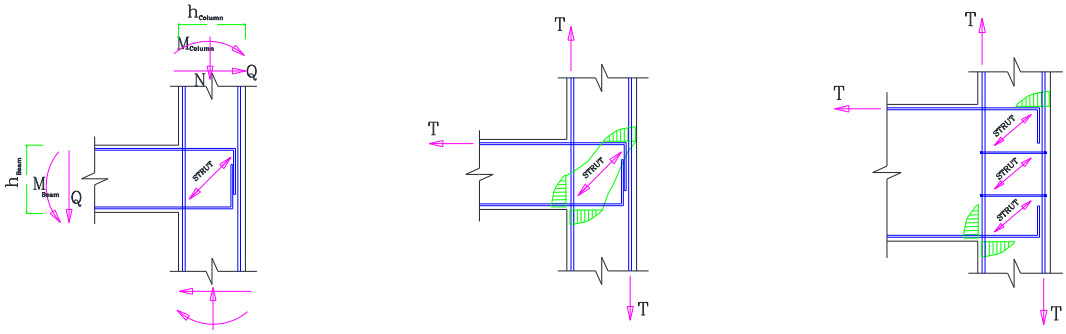

a)Forces acting on joint b) Formation of compression strut within joint c) Provision of additional ties to support multiple struts at shallow angle

Fig. 2: Additional transverse reinforcement, for large joint aspect ratio, Ref. [1,7,8]

In this paper, structural behaviors of beam-column joints with using steel shape in the joint zone were investigated and compared with conventional reinforced concrete beam-column joint specimen. The influence of different parameters, (including concrete-encased composite columns with IPE (I) and Pipe (P) steel sections. as well as, concrete-encased composite beams with Tee (T) and built up I sections with unequal flange width in the joint zone), on the ultimate strength, rigidity, and energy dissipation ability, etc., are investigated.

II. Experimental Program

2.1. Test Parameters

The main parameters examined in the experimental program are the following:

1. For columns, different steel shapes sections of equal cross-sectional area were used, i.e., I (IPE 100) and P (Pipe of diameter 120mm with 3mm thickness).
2. For beams, using different steel shapes sections with same depth, (150mm), and 600mm length, i.e., T shape with different flange width (110, 130 mm) and I shape with equal /unequal flange width (120/120, and 100/75).
3. Axial loading (N = 430 kN), calculated based on ACI-318 [1].
4. Joint zone with different connection details, (beam reinforcement embedded in column, using U shape bars for substituting cutting beam bars, and open stirrups at intersection zone between steel shapes of beam and column).
5. The dimensions, reinforcement, and steel sections of columns, beams, and joint details are shown in Fig. (3).

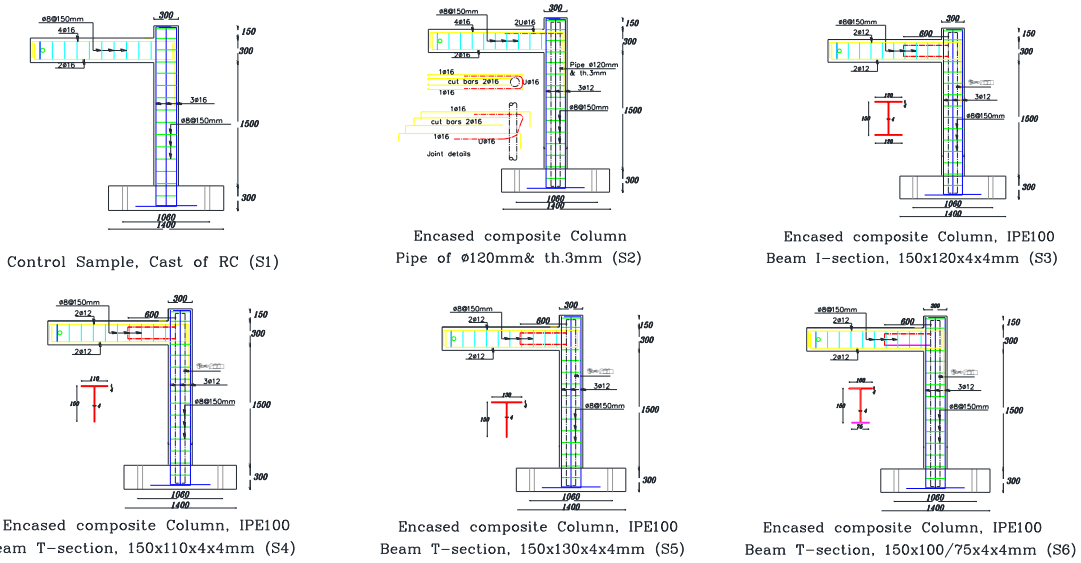

Fig. 3: The dimensions, reinforcement, and steel sections of columns, beams, and joint

2.2. Test Specimens

Six samples of beam-column joint with different steel shaped sections embedded in columns and beams are used in this study. Sample "S1" is monolithic reinforced concrete. It is the control sample, where the beam reinforcement embedded in column with stirrups (transverse reinforcement bars) in the joint zone. The samples were designed to represent approximately a model of a prototype beam-column used in special moment frame buildings. The test specimens had a rectangular cross section of 200×300 mm. Figure (4) stated the three configurations of cross sections for columns. Figure (5) illustrated the six configurations of cross sections for beams. The variables studied included use of different steel sections shapes in beam with equal / unequal flanges area, i.e., built-up T-section and I sections with different flange width. Different joint details include U shape bars for substituting cutting beam bars in S2 sample, and closed stirrups at intersection zone of beam and column through welding in encased steel sections, in samples S3, S4, S5, and S6). Fig. (3) summarized the test specimens. It has the same capacity of axial load ($0.3P_n$), as mentioned in Ref. [5]. It is used to distinguish the differences in seismic behavior for different beam-column connections. The magnitude of applied axial loads was chosen as 0.30 of the nominal axial compressive strength (P_n), (430kN), for an encased composite column, Ref. [1]. The (P_n) is limited to 0.8 the column capacity under uniaxial compression (0.8 P_0) to consider the effect of eccentricity. The ultimate loads (P_u) is limited to (φP_n), where resistance factor for compression equal to (φ = 0.70), as shown in Table (1).

$$P_0 = 0.85 \times f_c' \times A_c + f_{yr} \times A_r + f_{ys} \times A_s \qquad (1-a)$$

$$P_n = 0.8 \times P_0 \qquad (1-b)$$

$$P_u = 0.70 \times P_n \qquad (1-c)$$

Where:

f_c = Concrete compressive strength, 25MPa.

f_{yr}, f_{ys} = Yield strength of reinforcement bar, 360MPa, and steel sections, 270MPa, respectively.

A_c, A_r, A_s = Area of concrete, reinforcing bars, and steel shape respectively.

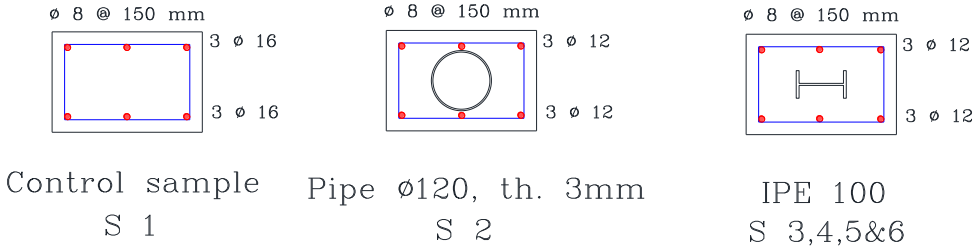

Fig. 4: The cross sections and reinforcement of columns samples

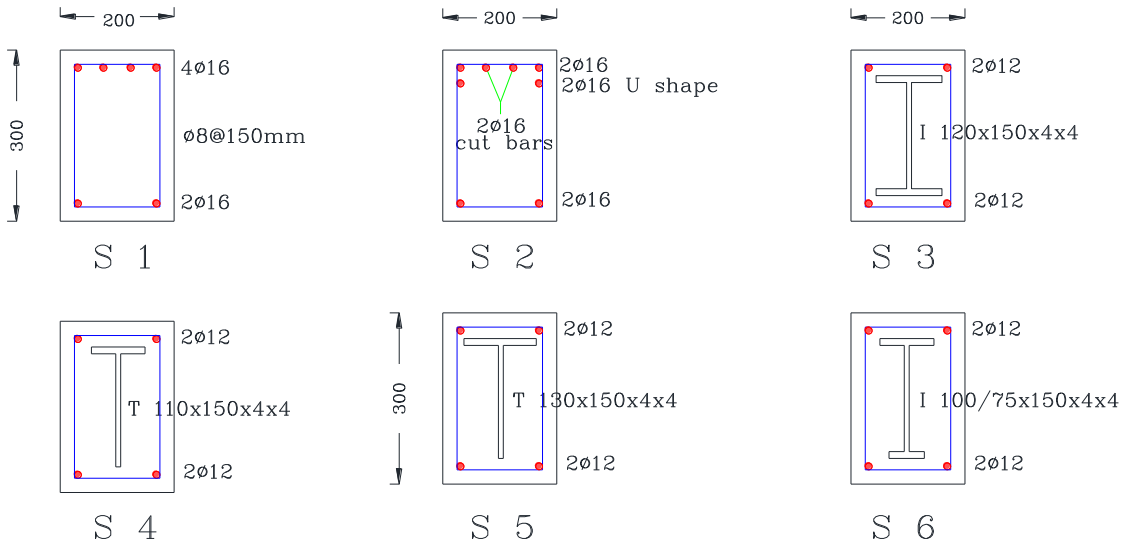

Fig. 5: The cross sections and reinforcement of beams samples

Table (1): The magnitude of applied axial loads equals to 430kN (0.30Pn) for an encased composite column, according to [5].

Specimen	Reinf.,	(A_c -(A_r+A_s))	A_r	A_s	A_r/A_c	P_o (N)	P_n (N)	P_u (N)	n (ratio)
Conc. Sample	6ϕ16	58793	1207	0	2.01%	1733797	1387038	970926.3	0.31
Pipe sample	6ϕ12	58218	679	1103	1.13%	1828855	1463084	1024159	0.29
IPE sample	6ϕ12	58291	679	1030	1.13%	1810723	1448578	1014005	0.30

2.3. Material Property

The beam-column joints were constructed and tested at Reinforced concrete lab in NHBRC. All specimens were tested after 6 months of casting due to late of fixing the crane in lab. The used concrete was mixed in batching plant of the lab. To determine the average concrete compressive strength three cubes (150×150×150 mm) were tested for each specimen. The measured concrete compressive strength was around 35 MPa, (equivalent to cylinder compressive strength 26 MPa). The average values of the steel mechanical properties were determined through testing three samples of reinforcing steel bars for each nominal diameter, but for steel section the given values of the factory were taken. Table (2) illustrates the obtained testing values.

Table (2): Material properties for steel sections and reinforcing bars

Material	Yield strength, f_y (N/mm^2)	Ultimate strength, f_U (N/mm^2)
Stirrups Ø 8	317	410
Bars Φ 16 & Φ 12	360	516
IPE100 & Pipe φ120	270	411

2.4. Test Set-up

The whole test set-up for cyclic loading is as shown in Fig. (6). Each specimen was fixed to the floor of the laboratory through anchorage concrete block. The anchorage block of the specimen is fixed to the laboratory floor with pre-stressing steel bars to prevent uplifting of the specimen during the application of the cycling loading. For each specimen, an axial load was applied on the column with hydraulic jack. The axial compressive load was applied at the upper end of column and it remained constant. The beam-column specimens were subjected to a uniform compression load equals to 0.30 P_n, during application of cyclic vertical loading on the end of the beam. Up and down cyclic loading on the end of the beam was applied with hydraulic actuator. The cyclic hydraulic actuator has a capacity of ±250kN (compression & tension). The lateral load was applied by a servo-controlled hydraulic actuator at the end of the beam, using a displacement-controlled testing at a speed of 10 mm/min. Moreover, a blocking mechanism involving a truss frame is used for preventing the horizontal sliding of the specimen.

Test Set-up

2.5. Verification of Proposed Set-up

The joint is (T) type for simulating the edge beam-column joints in frame structures. The joint aspect ratio (h_{beam} / h_{column}) is close to 1.0, to develop the compression strut across the joint. As shown in Fig. (7), the straining actions represent the actual forces that acting on the joint in special moment frames during earthquakes. In other words, the setup is able to develop the shear forces that acting on the joint due to moment transfer at beam-column joints. Therefore, the proposed setup is adequate to investigate the behavior of the different types of suggested connections in the joint zone during this study.

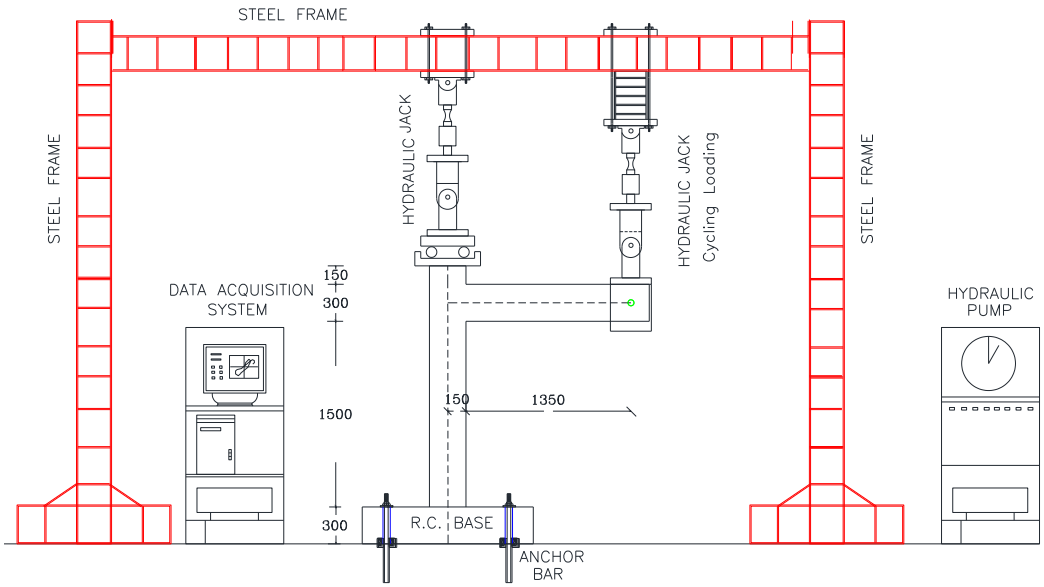

Fig. 6: Test set-up for cyclic loading test

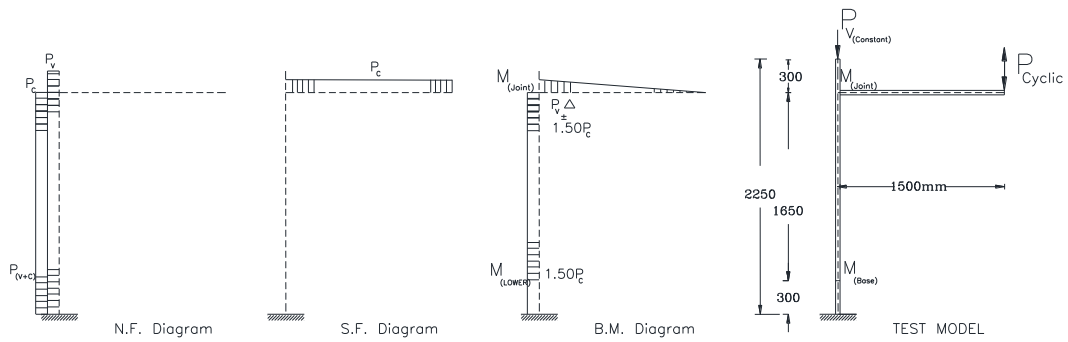

Fig. 7: The set-up is adequate to investigate the shear capacity of edge beam-column joint.

2.6. Instrumentation

The data acquisition system consists of six internal control and recording channels for monitoring data from external instruments [linear variable displacement transducers (LVDTs)]. In addition to the load cells at the end of the hydraulic actuators, a series of LVDTs were used for measuring critical response quantities. As shown in Fig. (8), one LVDT was installed at the end of the beam to monitor the cyclic displacement. A second one was installed at the base to measure the sliding of the base. Two further LVDTs, close to the boundary elements, were installed on both sides of the column to measure the axial deformations. Finally, two further LVDTs, were installed diagonally on the joint zone to recognize the strut deformation under reversal loads. The foregoing system of measurements made it possible to estimate the flexural, shear, and sliding components of the specimen deformation, as discussed in the following sections.

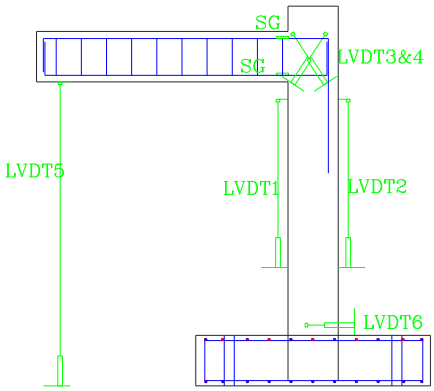

Fig. 8: Instrumentation of Typical Specimens.

2.7. Application of Cyclic Loading

The cycling (reversal) loading was applied at the end of the beam, Fig. (6). Displacement control was used throughout the test, with the exception of the first cycles in the elastic range. The typical displacement history, up to the failure point, defined as that corresponding to 75 percent of the maximum strength. The beam-column joints were laterally subjected to a predetermined cyclic displacement history as indicated in Fig. (9a,b). Cyclic displacement of equal positive and negative displacement was used for samples (S1, S2, S3, and S6). Referring to ACI 318, Ref. [7], allowing use of half the (–ve) reinforcement at support in lower side of the section to resist reversal loads generated from earthquakes. The (–ve) moment of beam at support is generated from dead, live, and lateral loads while the lower side affected only by the moment generated from lateral loads. Therefore, cyclic upward displacement equal to half downward displacement was used for samples with T section steel shapes, (S4, and S5), as well as, for sample S2, as shown in Fig. (9b). The axial load, that applied on the column, was equal to 0.30 P_n during the entire test. Fixed connection at the tip of the vertical actuator allows for framing behavior of samples. Load-lateral displacement hysteresis curve and the state of structural steel strain were observed to judge whether the specimen is yielded.

III. Test Results

3.1. Hysteretic Curves for Specimens

Hysteretic curve is a load-displacement relationship curve of the specimen under cyclic loading, which is the important presentation of seismic performance. As shown in Fig. (10), the hysteretic curve is described by the measured cycled load and displacement at the end of the beam. All the specimens have some hysteretic characteristics in common: at the early stage of loading, the specimens are in elastic stage and a linear relationship between load and displacement is presented. Tensile cracks were formed at the interface between column and beam. The loading curve coincides with the unloading curve. With the increasing of load, the curve deviates from a straight line. After cracking of beams, the specimens enter into the elastic-plastic stage. In few samples, a clear vertical split at the junction were formed. The residual deformation exists in unloading process and the area of hysteresis loop increases gradually. In addition to this, there were hair cracks in the joint region.

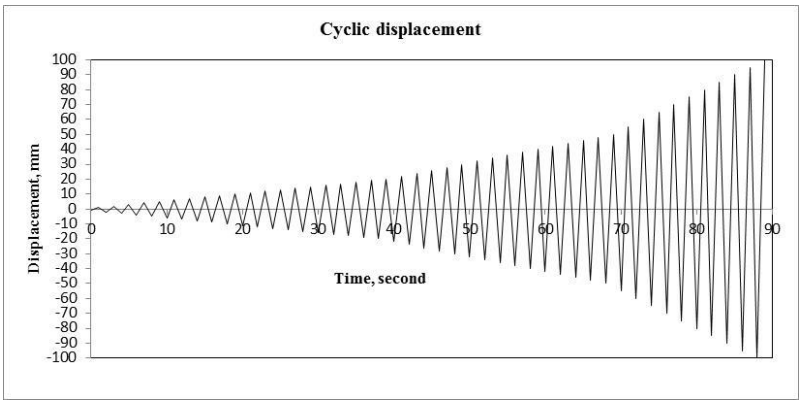

Fig. 9a: A typical Sequence of Displacement Cycles, with equal ±ve values, for beams with both I built up sections and reinforcement bars.

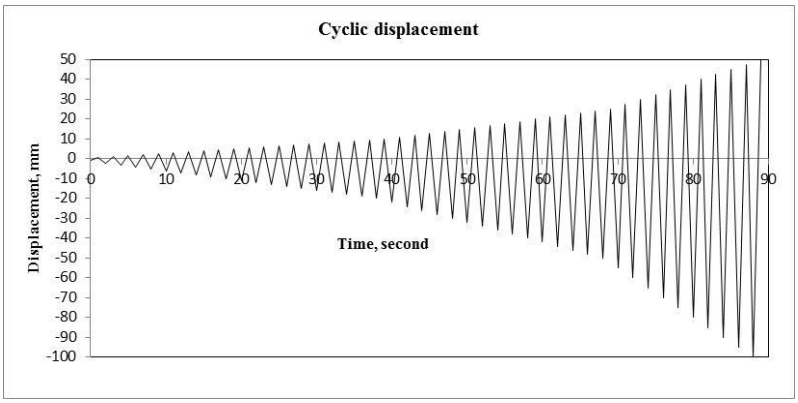

Fig. 9b: A typical sequence of displacement cycles, with unequal ±ve values, for encased beams with T built up sections.

The ultimate load capacity of specimen S3 and S6, (I steel section) for downward and upwards loads, was 34% and 14% lower than that of S1, (concrete control sample). By studying the cracking pattern of the three samples, it is recognized that only tinny hair cracks formed in both samples S3 and S6. In other hand, shear cracks are formed in the joint zone of S1. The failure of both samples S3 and S6 was due to shear failure of beam at end of encased steel I section zone. This mode of failure was referred to sudden change of beam stiffness. Therefore, it is advised to extend the encased steel section till inflection point of moment in beam. Added to that, the application of Steel shape sections in the joint zone improves the joint shear strength due to confinement of concrete.

The ultimate load capacity of specimen S4 and S5, (T steel section) for downward loads, is 38% lower than that of S1, (concrete control sample). The explanations of obtained results were the same as discussed above for samples S3 and S6.

3.2. Crack Pattern and Failure Mode

Failure modes of beam-column joint without/with shaped steel section include the tensile rupture of beam reinforcement, splitting of concrete occurred at the base of the beam, and brittle shear failure of concrete in either beam or joint zone. The failure types are shown in figure (11).

For sample S1, the bending cracks appear at 7 to 9 mm displacement at upper and lower beam faces. Both upper and lower cracks connected together at 12 to 14 mm displacement. With further increase of the external load intersectional shear cracks occurred in the beam zone. Finally, it failed by brittle shear failure of concrete in beam zone at 48mm displacement.

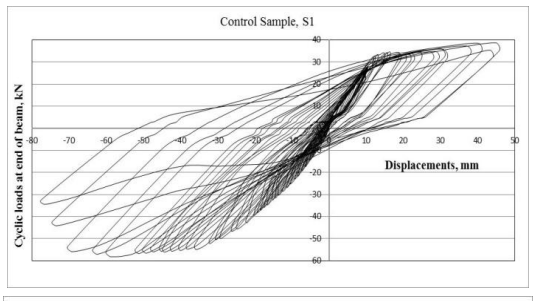

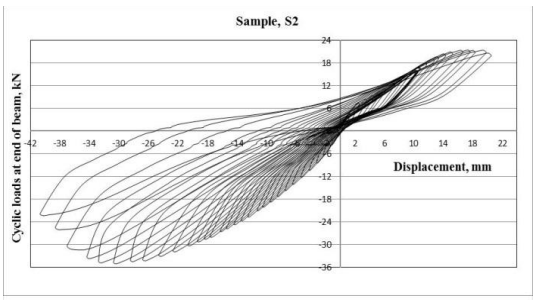

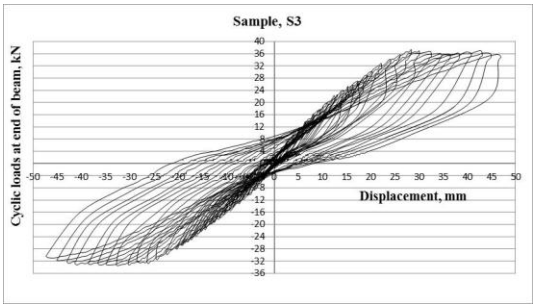

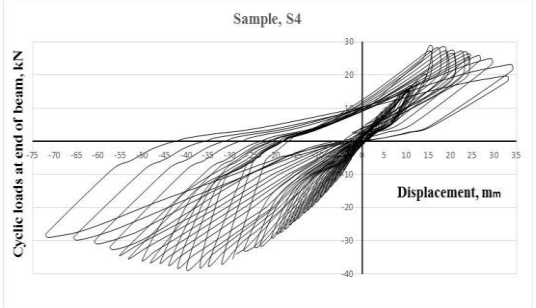

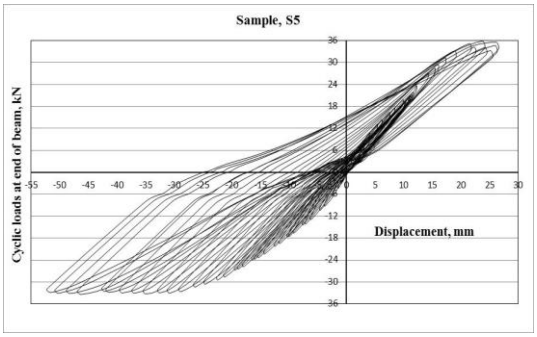

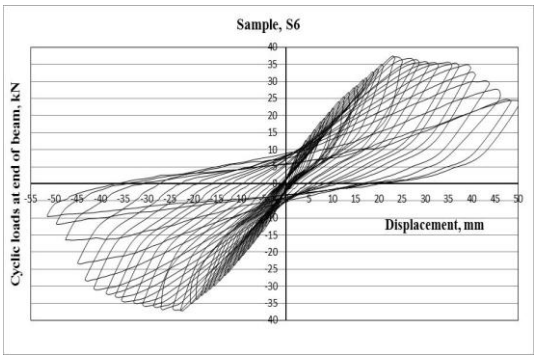

Fig. 10: The displacement versus Lateral loads hysteresis loops

a) S1, shear failure attached with spalling of concrete due to yield of bottom reinforcement

b) S2, shear failure at joint zone combined with yielding column reinforcement

c) S3, brittle shear failure of concrete at end of encased steel section in beam zone

d) S4, bending failure full development of plastic hinge at the base of the beam

e) S5, shear failure of concrete at end of encased steel section in beam

f) S6, shear failure in RC at end of encased steel section in beam

Fig. 11: Failure modes of Beam-Column joints with/without steel shaped sections

For sample S2, the bending tinny cracks appear at 10 to 14 mm displacement at upper and lower beam faces. Intersectional shear cracks occurred in the joint zone at 14 to 15 mm displacement. With increasing displacement, more shear cracks occurred in the joint zone combined with longitudinal column cracks due to less concrete cover at crown of embedded pipe in column. Finally, specimen S2 failed at a displacement of 36 mm due to shear crack of concrete at joint zone and yielding of longitudinal column reinforcement.

In S3 sample, few flexural cracks appeared in the height of 600 mm from the base of the beam at displacement 7 to 12mm. The cracks extended to the center line of the beam at 24mm displacement. A full crack occurred at the interface between beam and joint at displacement equal to 13 to 17mm. With increasing displacement, shear cracks occurred in the joint zone at displacement 18 to 24mm. With further increase of the external load, Intersectional shear cracks occurred at end of encased I steel section in the beam accompanied with spalling of concrete cover due to widening of shear cracks and excessive deformation of bottom reinforcement. Finally, S3 failed by brittle shear failure of concrete at end of encased steel section in beam zone at 43 mm displacement.

For S4, the initial tiny crack occurred at the interface between beam and joint, as well as, along 900mm of beam base. The cracks extended to near the center line of the beam. Shear cracks occurred in the joint zone at displacement 48 to 70 mm. A major flexural crack formed at the base of the beam at displacement of 52 mm. The flexural cracks concentrated near the base of the beam where yielding of steel reinforcement occurred. Finally, failure of S4 was caused by full development of plastic hinge at the base of the beam at 70 mm displacement.

In sample S5, a tinny crack occurred at the interface between beam and joint at displacement equal to 9 mm. Group of ductile cracks at lower and upper side of beam at displacement ranged from 12 to 14 mm. The ductile cracks joined at displacement of 14 to 24 mm. With further increase of the external load, intersectional shear cracks occurred at end of encased T steel section in the beam at displacement 24 to 32 mm. Shear cracks became more widening at 36 to 46 mm. Shear cracks occurred in the joint zone at displacement 46 mm. Finally, S5 failed by brittle shear failure of concrete at end of encased steel section in beam zone at 46 mm displacement.

For S6, a crack occurred at the interface between beam and joint at displacement equal to 9 mm and connected at 15 mm. Spread of ductile cracks at lower side of the beam at displacement ranged from 17 to 20 mm. The ductile cracks joined at displacement of 24 to 26 mm. With further increase of the external load, shear cracks occurred at end of encased I steel section in the beam at displacement 27 to 30 mm. Shear cracks became more widening at 36 to 46 mm. No shear cracks occurred in the joint zone till end of test. Finally, S6 failed by brittle shear failure of concrete at end of encased steel section in beam zone at 42 mm displacement.

3.3. Skelton Curve

The skeleton curve reflects the characteristic of stress and deformation at different stages of specimens, which is the important basis to determine the feature point in restoring force model. In analysis of skeleton curve, negative loading direction is defined when the hydraulic actuators pull the specimen in downward

direction, while positive loading direction is defined when the hydraulic actuators push the specimen in upward direction. Figure (12) shows the envelope curves for the six samples.

It is realized that, for samples S4 and S5, (T steel shape has the same depth 150mm, with different flange width 110, 130 mm and 600mm length), the ultimate loads ranges from 36 to 38 kN, while the maximum displacement ranges from 52 to 72 mm.

For samples S3 and S6, (I steel shape has the same depth 150mm, 600mm length and has different flange width 120*120, and 100*75 mm and), the ultimate loads ranges from 37 to 46 kN, while the maximum displacement ranges from 46 to 48 mm.

From curves of S1 and S2, (S1 has 6 bars of 16mm diameter, S2 has a pipe of diameter 100mm and 3mm thickness), the ultimate loads ranges from 35 to 44 kN, while the maximum displacement ranges from 38 to 72 mm.

It is obvious that, the samples with I section, (S3 and S6), give higher ultimate loads than Samples with T section, (S4 and S5) by maximum 21%, while the maximum displacement reduced by 33%. Comparing to control samples, (S1 and S2), the samples with I section, (S3 and S6), had higher ultimate loads by 4.5%. In the same time, it has lower displacement by 33%. On the other hand, the samples with T section, (S4 and S5), had lower ultimate loads by 13.60%, But they had the same displacement.

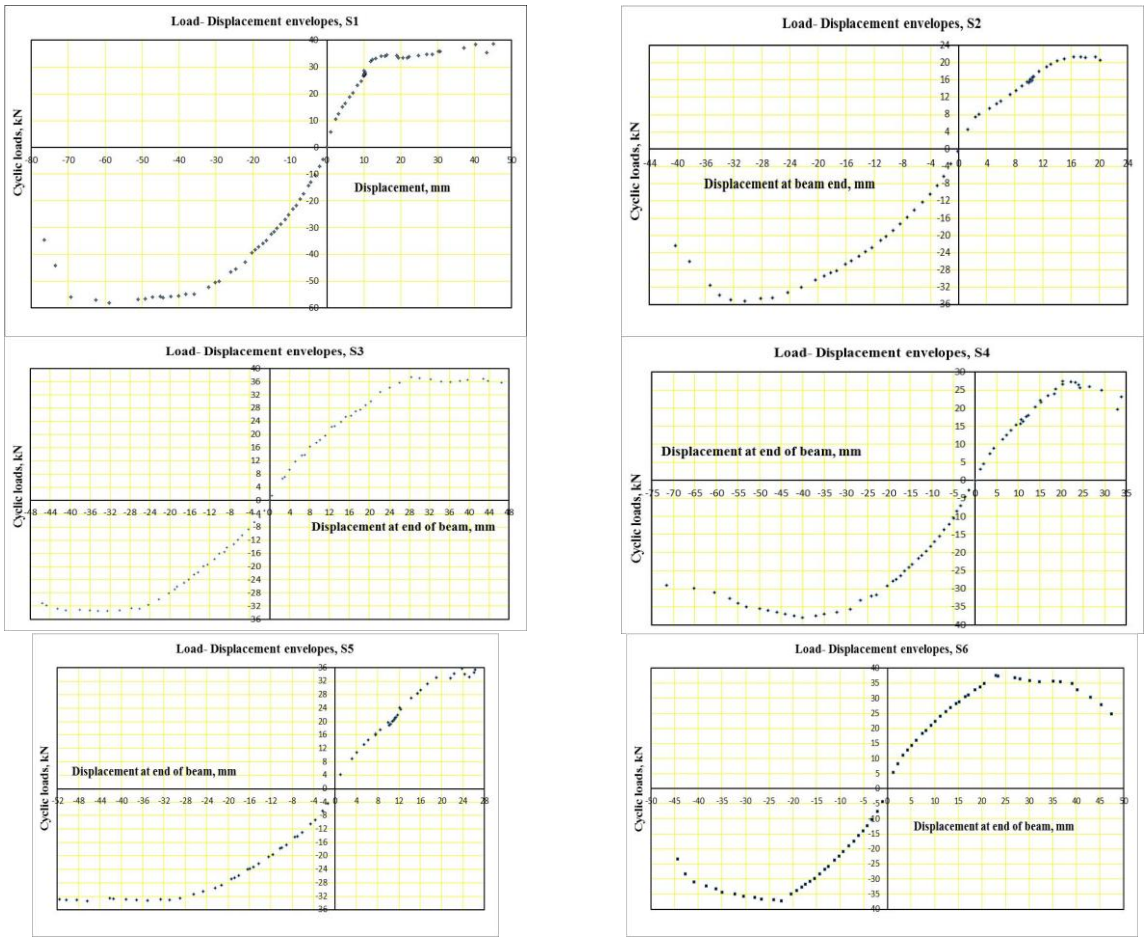

Fig. 12: The skeleton curves for all specimens

3.4. Ductility Coefficient

Ductility is an important index of structural seismic behavior. It is the ability of the structure to sustain large deformation and a capacity to absorb energy by hysteretic behavior, as mentioned in Pauly & Priestly, Ref. [10]. To evaluate deformation capacity of specimens, a displacement ductility ratio is adopted. As shown in Fig. (13), the yield point is the deviation point of the envelope curves tangent that drawn from origin point. The maximum (failure) load is based on the greater load value which falls to 85% of the ultimate load, Ref. [2,5, &10] or the load at the sudden failure of the specimens. The ductility μ is defined as the ratio of displacement at failure load to displacement at yielding load of the sample.

$$\mu = \frac{\Delta_{max}}{\Delta_{yield}} \qquad (2)$$

The values of P_u (ultimate load), P_y (yielding load), Δ_y (displacement at yielding load), Δ_{max} (displacement at failure load), and μ (ductility ratio) are illustrated in Table (3). They were calculated from the envelope curves for the positive and negative loading. From the table, it is realized that:

1- The yielding point was determined based on Paul and Pristly, (= $0.85\times0.7\times P_u$), Ref. [10].
2- All joint of beams with encased I steel sections have ductility coefficient μ ranges from 3.80 to 4.61. It had a narrow deviation from maximum and minimum values equal to 0.4.
3- All joint of beams with encased T steel section have ductility coefficient μ ranges from 2.94 to 5.97, But it had a wide deviation from maximum and minimum values equal to 1.52.
4- Compared to maximum displacement of control specimen S1, joint of beams with encased I section gives higher displacement ratio than beams with encased T section,
5- The sample S2 with U bars, (substituting cut bars), had the lowest ductility coefficient, (2.8 to 3.2) and displacement ratio of all connection types.

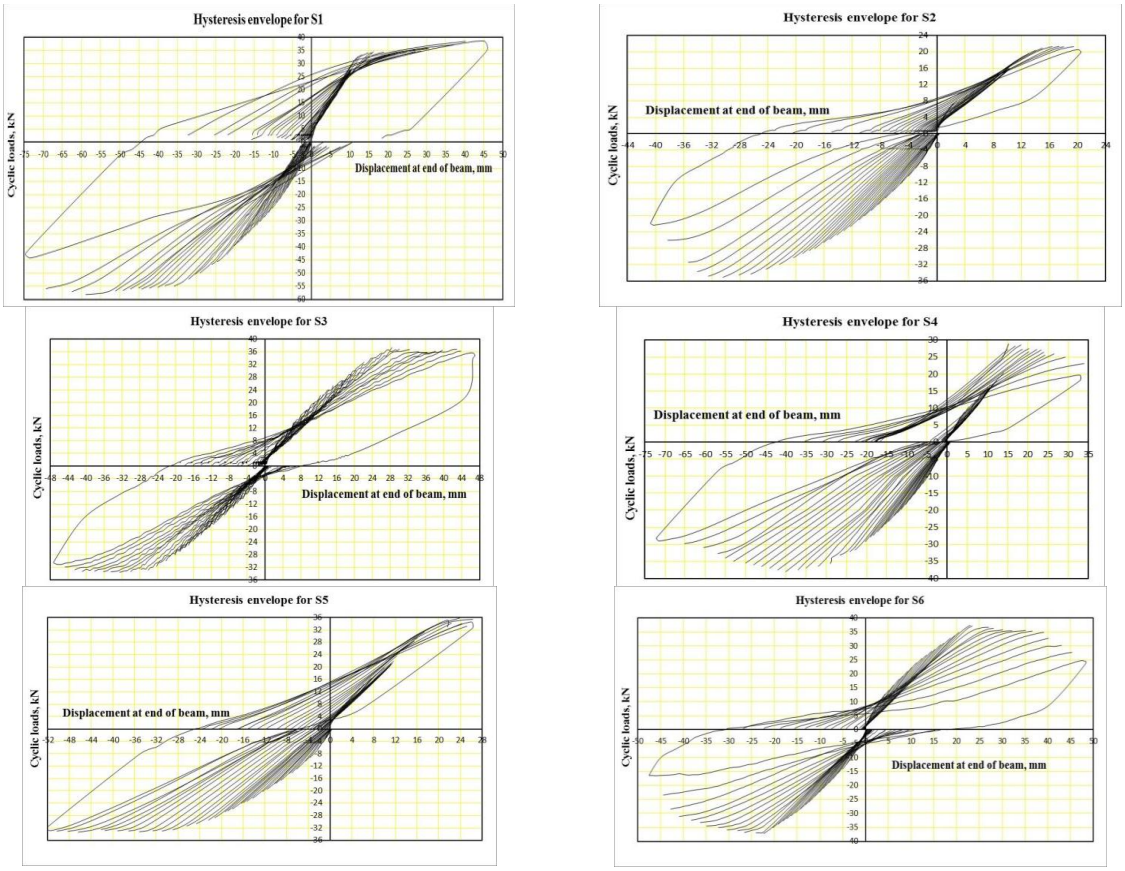

Fig. 13: The hysteresis envelope curves for positive and negative loading.

3.5. Energy Dissipation

Equivalent damping coefficient η_e is an important parameter for evaluating the energy dissipation capacity of beam-column joint specimens. Equivalent damping coefficient can be calculated according to the hysteresis loops in Fig. (14), and can be expressed as the areas enclosed by the loop of hysteresis curve, which denote the inelastic dissipating energy in one complete hysteresis loop. The analysis of energy dissipation capacity adopts equivalent viscous damping coefficient η_e by the following equation, Ref. [9].

$$\eta_e = \frac{1}{2\pi}\frac{A_{(abd+cdb)}}{A_{(Oia+Ojc)}} \qquad (3)$$

Where:

$A_{(abd+cdb)}$: Area of load displacement hysteretic loop at maximum load, for both ascent and descent parts.
$A_{(Oia+Ojc)}$: Area of triangles for both ascent and descent of loop at maximum load.
The area of triangles represents the maximum energy, i.e.,

$$E = P\times \Delta / 2 \qquad (4)$$

Table (3): Ductility ratio μ and its percentage to control sample

Sample	Case of loading	P_y	Δ_y	P_u	Δ_u	$P_{failure}$	Δ_{max}	$\mu=\frac{\Delta_{max}}{\Delta_y}$	$\frac{\Delta_{Sample}}{\Delta_{S1}}$
S1	Down (-ve)	34.5	13	58	59	49	73	5.62	1.0
	Up (+ve)	22.5	8	39	45	39	45	5.63	1.0
S2	Down (-ve)	21	11.5	35	31	29.5	37	3.22	0.51
	Up (+ve)	12.6	7.5	21.20	18.5	20	21	2.80	0.47
S3	Down (-ve)	19.25	12	34	33	30	47	3.92	0.64
	Up (+ve)	21.25	12.5	37.25	29	36	47.5	3.80	1.06
S4	Down (-ve)	22.75	13	38.5	40	32.5	58	4.46	0.79
	Up (+ve)	17.2	9	29	16	24.6	29	3.22	0.64
S5	Down (-ve)	19.6	8.8	33.8	46.5	32	52.5	5.97	0.72
	Up (+ve)	21.3	9	36	24	34	26.5	2.94	0.59
S6	Down (-ve)	22	9.5	37.6	23	31.9	41	4.32	0.56
	Up (+ve)	22	9	37.5	23	31.8	41.5	4.61	0.92

Table (4): The equivalent viscous damping coefficient η_e

Sample	**Area of max. hysteresis loop**	**Area of max. energy (area of triangles)**	**Viscous damping coefficient(η_e)**
S1	2960.661	2494.3356	0.1888
S2	338.4156	740.5007	0.0727
S3	1116.967	1487.993	0.1194
S4	667.0187	1014.953	0.1046
S5	718.5483	1239.56	0.0922
S6	293.6392	846.8925	0.0552

Figure (14) shows the maximum hysteresis loop that used in calculating viscous damping coefficient ηe. The equivalent viscous damping coefficient, ηe, is illustrated in Table (4). The results demonstrate that joint of beams with encased I and T shaped steel section (S3, S4, &S5) have favorable seismic behavior and good energy dissipation capacity than joint of both beams with narrow flange width (S5), and, beams with cut bars (S2).

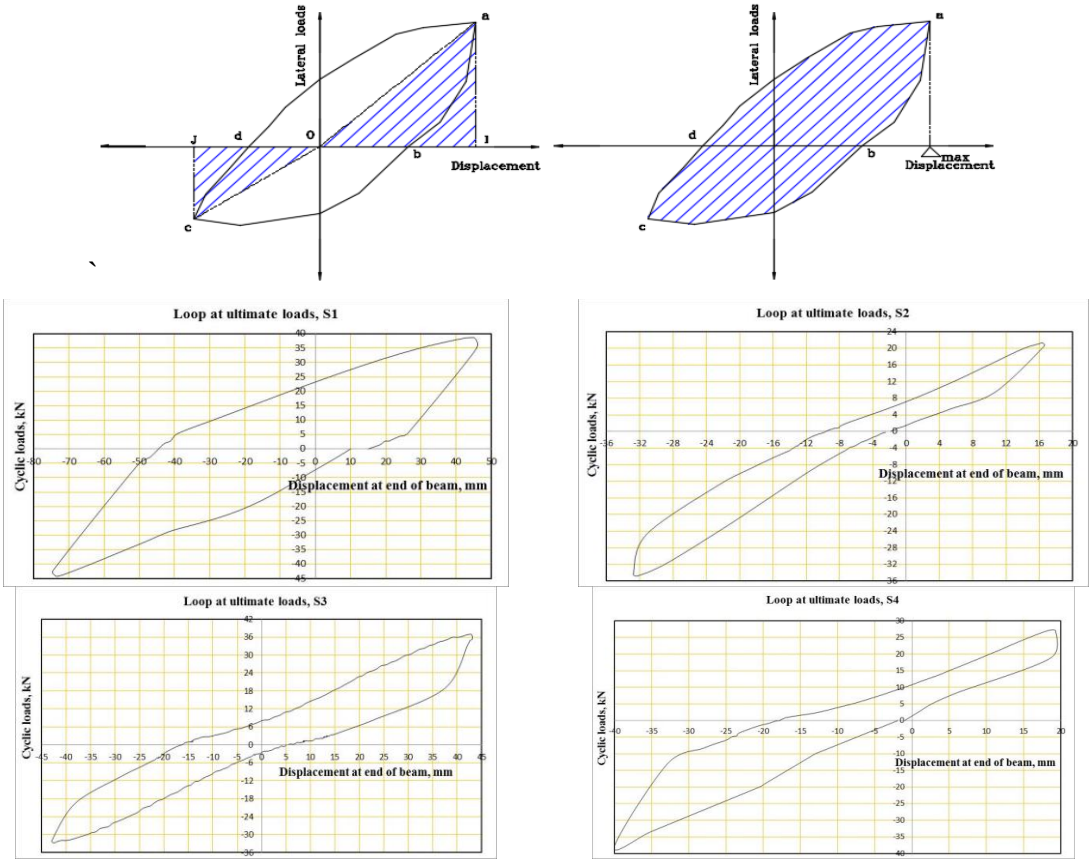

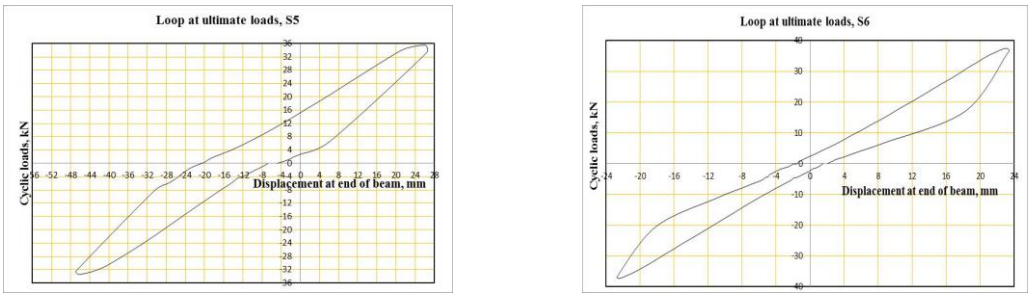

Fig. 14: The maximum hysteresis loop for calculating viscous damping coefficient η_e

IV. Conclusions

In the present paper, a number of beam-column joint specimens with different configurations have been tested to investigate the seismic behavior of joint zone. The beam was strengthened by using different steel sections, (built-up T-section and I sections had different flange width), as well as, the columns were composite with encased IPE100 steel section. There were two samples of reinforcing concrete, but one of them has a composite column with encased pipe section of diameter 120mm and the beam has a U shape bar for substituting cutting bars that faced the pipe section at the joint zone.

- The ultimate load capacity of specimen with both T and I steel section were lower than the obtained one of the control specimens. The failure of samples with (T and I) were due to shear failure at end of encased steel sections, due to sudden change of beam stiffness. In the same time, there were only one or two tiny cracks in joint zone despite there were cross cracks spread in the joint zone of control sample. Therefore, the encased steel section is advised to extend till inflection point of moment in beam. Added to that, the application of steel shape sections in the joint zone improves the joint shear strength due to confinement of concrete.
- From Skelton curves, it could be concluded that, the samples with I section, (S3 and S6), give higher ultimate loads than samples with T section, (S4 and S5) by 21%, while the maximum displacement reduced by 33%. On the same manner, the samples (S3 and S6) had higher ultimate loads by 4.5% than control sample S1, but they had lower displacement by 33%.
- From Table (4), the beams with encased T section have ductility coefficient μ ranges from 2.94 to 5.97, while, beams with encased I sections have μ ranges from 3.80 to 4.61. Compared to maximum displacement of control specimen S1, joint of beams with encased I section gives higher displacement ratio than beams with encased T section. The sample (S2) with U bars, (substituting cut bars), had the lowest ductility coefficient, (2.8 to 3.2) of all connection types.
- Based on Figure (14), beams with encased I and T shaped steel section (S3, S4, & S5) have favorable seismic behavior and good energy dissipation capacity than joint of both beams with narrow flange width (S5), and, beams with cut bars (S2).

Finally, it obvious from experimental results that, using of composite steel sections at joint zone minimize the cracks, and lead to weak beam- strong column design criteria, as well as, improves its seismic behavior.

References

[1]. Y. C. Choi, et al. "Development of a shear strength equation for beam-column connections in reinforced concrete and steel composite system". *International Journal of Concrete Structures and Materials, Vol.11:* pp.185-197, (2017).
[2]. E. Z. Beydokhty, and H. Shariatmadar. "Behavior of damaged exterior beam-column joints strengthened by CFRP composites". Latin American Journal of Solids and Structures, Vol.13: pp.880-896, (2016).
[3]. H. Khalil, et al. "Investigation on an innovative way to connect RC beam and steel column". International Journal of Civil and Enviromental Engineering, Vol.4: pp.437-443, (2015).
[4]. K. R. Bindhu, P. M. Sukumar, and K. P. Jaya. "Performance of exterior beam-column joints under seismic type loading". ISET Journal of Earthquake Technology, Vol.46 No. 2: pp.47-64, (2009).
[5]. J. L. Pan, and F. YUAN. "Seismic behaviors of ECC/ Concrete composite beam column joints under reversed cyclic loading". VIII International Conference on Fracture Mechanics of concrete and concrete structures: 1-12, (2004).
[6]. W. Kim, and L. W. LU. "Hysteretic analysis of composite beam to column joints". Earthquake Engineering, 10th World Conference, Balkema, Rotterdam: 4541-4546, (1992).
[7]. ACI318-14. "Building code requirements for structural concrete (ACI 318M-14) and commentary (ACI 318RM-14)". ACI standard, American concrete Institute, Farmington Hills, (2014).
[8]. S. K. Ghosh. "Significant changes from the 2011 to the 2014 edition of ACI 318". Precast/Pre-stressed Concrete Institute, c/o PCI Journal, 200 W. Adams St., Suite 2100, Chicago, IL60606:56-79, (2016).
[9]. S. Watson, et al. "Investigation on an innovative way to connect RC beam and steel column". ACI Journal of Structural Engineering, 120(6): pp.1798-1823, (1994).
[10]. Paulay, and M. Priestley. "Seismic design of reinforced concrete and masonry buildings". John Wiley and Sons, New York, (1992).